An investigation of characteristics of airblast atomization using 3D DNS for altitude relight conditions

Anirudh Asuri Mukundan, Thibaut Menard, Alain Berlemont, Jorge César Brändle de Motta

11th U.S. National Combustion Meeting
Organized by the Western States Section of the Combustion Institute
March 24–27, 2019
Pasadena, California

An investigation of characteristics of airblast atomization using 3D DNS for altitude relight conditions

Anirudh Asuri Mukundan[1,*], *Thibaut Ménard*[1], *Alain Berlemont*[1], *and Jorge César Brändle de Motta*[1]

[1]*CNRS UMR6614-CORIA, Rouen, France*
[*]*Corresponding author:* anirudh.mukundan@coria.fr

Abstract: This paper presents results from direct numerical simulations (DNS) of planar pre-filming airblast atomization. The liquid/gas interface has been captured using coupled level set moment of fluid method. This method is a hybrid between moment of fluid and coupled level set volume of fluid methods. The numerical method has been applied to airblast atomization analyzed experimentally by Gepperth et al. (2012, "Ligament and Droplet Characteristics in Prefilming Airblast Atomization", ICLASS 2012). The operating point investigated in this work correspond to aircraft altitude relight condition. The post-processing of the DNS data is performed consistently with that for the experimental data. The main mode of breakup observed is torn sheet breakup. A good agreement was found between simulations and experiments for Sauter Mean Diameter and droplet streamwise velocity distribution while satisfactory agreement has been found for the droplet diameter distribution and ligament breakup length.

Keywords: ***Airblast, Atomization, Relight, DNS, CLSMOF***

1. Introduction

With the increasing air traffic, there has been increasing regulations on pollutant emissions from aircraft engines. In order to meet these regulations, lean combustion strategies are being employed. The primary prerequisite for success of this strategy is the high quality mixing between fuel and air. To this end, pre-filming airblast atomization technique has been commonly used in aircraft engines. In these atomizers, a thin liquid fuel film is formed on the pre-filmer plate which is then disintegrated into droplets by shearing mechanism of the gas flowing above and below the plate. Since atomization process controls the effective fuel-air mixing which in turn affects the combustion efficiency and pollutant emissions, it is imperative to study this process in order to get better control of it.

With the idea of airblast atomization first introduced by Lefebvre and Miller [1], there has been multiple experimental investigations [2, 3] to understand the physical processes of atomization occurring in the atomizing edge. Most of these experimental analysis focused on the far downstream properties such as droplet diameter and velocity distribution analysis. But the characteristics of atomization near the pre-filmer plate have not been extracted from experiments. The work of Bilger and Stewart Cant [4] focused on the airblast atomization and regime classification for different gas and liquid phase velocities. This work used laminar velocity profile for the phases thus might not necessarily represent the real time fuel injection scenarios. Recently, the works of Gepperth et al. [5] and Warncke et al. [6] on planar pre-filming airblast atomization extracted experimentally and numerically the information close to the plate such as ligament lengths and deformation velocity. Although a good agreement between experiments and simulations had been observed in the work of Warncke et al. [6], the results displayed the limitation of the diffused interface capturing methods used in their simulations.

Thus, to this end, in our work we have used direct numerical simulations (DNS) approach to simulate the planar pre-filming airblast atomization for same operating point and configuration as described in Warncke et al. [6] and compare the results with the experimental work of Gepperth et al. [5]. In contrast to Warncke et al. [6], we use a sharp interface capturing method called coupled level set moment of fluid (CLSMOF) method for accurately capturing the

liquid/gas interface. This method is a combination of conventional moment of fluid (MOF) method [7, 8] and coupled level set volume of fluid (CLSVOF) method [9].

This paper is organized as follows: after summarizing the governing equations in Section 2, the numerical method of CLSMOF is presented in Section 3. This is followed by the presentation of the case setup and configuration of the airblast atomizer used in this study. Finally, the results from the DNS of airblast atomization are presented and discussed in Section 5.

2. Governing Equations

The solver used in this study is ARCHER, whose capabilities are described extensively in multiple works [9–11]. This solver is structured, parallel and developed for direct numerical simulations (DNS) of complex and turbulent multiphase flows with the application to study primary breakup of liquid fuel jet. A staggered variable configuration is used with central finite difference scheme for least numerical dissipation.

The pressure and velocity fields describing the flow are obtained by solving the incompressible Navier–Stokes equations. The following form of the Navier–Stokes equations are solved in ARCHER:

$$\underline{\nabla} \cdot \underline{u} = 0, \tag{1}$$

$$\frac{\partial \rho \underline{u}}{\partial t} + \underline{\nabla} \cdot (\rho \underline{u}\,\underline{u}) = -\underline{\nabla} P + \underline{\nabla} \cdot (2\mu \underline{D}) + \underline{B}, \tag{2}$$

where $\underline{u}$ is the velocity field, P is the pressure field, μ is dynamic viscosity, ρ is density, $\underline{D}$ is the strain rate tensor given as $\underline{D} = \frac{1}{2}(\underline{\nabla u} + (\underline{\nabla u})^T)$, and $\underline{B}$ is the sum of the body and surface tension forces. $\underline{B} = \underline{B}_{\text{b}} + \underline{B}_{\text{st}}$ where $\underline{B}_{\text{b}}$ is the force due to gravity and $\underline{B}_{\text{st}}$ is the force due to surface tension which is given as $\underline{B}_{\text{st}} = \sigma\kappa\delta_I \underline{n}$. σ represent the surface tension, κ is the curvature of the interface computed using the liquid/gas interface unit normal $\underline{n}$ as $\kappa = \underline{\nabla} \cdot \underline{n}$, and δ_I is the Dirac delta function centered on it. A consistent mass and momentum flux computation [11] is employed.

A projection method as described in Ménard et al. [9] is employed for solving Equations (1) and (2). A 2^{nd} order central difference scheme is employed for discretization of the spatial derivatives to avoid any dissipation. However, the convection term is discretized using 5^{th} order WENO scheme to ensure a robust behavior of the solution. A consistent mass and momentum flux computation [11] is employed. The viscous term is discretized following the method described in Sussman et al. [12]. Ghost Fluid Method (GFM) [13] is employed for the spatial discretization of the Poisson equation for taking into account the force due to surface tension as a pressure jump. The resulting linear system of symmetric and positive definite matrix with five diagonals is solved using multigrid algorithm for preconditioning a conjugate gradient (CG) method [10]. The temporal derivatives in this study are discretized using one-step forward Euler scheme.

3. Numerical Method

In this section, we first briefly summarize the coupled level moment of fluid (CLSMOF) method employed for liquid/gas interface capturing within the context of multiphase flows. Then the numerics behind the CLSMOF interface reconstruction and advection are presented. Finally, a criteria for distinguishing resolved and under-resolved interface is presented.

3.1 CLSMOF Method

Within the context of multiphase flows, it is imperative to accurately capture the liquid/gas interfaces. To this end, we have used CLSMOF interface reconstruction method. We have developed in our solver the CLSMOF method as a combination of conventional moment of fluid (MOF) [7, 8, 14, 15] and coupled level set moment of fluid (CLSVOF) [9] methods. This way, it is possible to combine the advantages of both methods: accurate capture of under-resolved liquid droplets from MOF and sharp interface representation from LS methods. The objective is to use a computationally more expensive MOF method only for reconstructing under-resolved liquid structures.

MOF method is a superset of conventional volume of fluid (VOF) method. MOF method tracks both liquid volume fraction (zeroth moment of liquid volume) and phase centroids (first moment of liquid volume) in each mixed computational cell (cell with non-zero liquid volume fraction) in order to numerically reconstruct the interface. A piecewise linear interface calculation (PLIC) method is used for reconstructing the interface. Thus, the equation of the reconstructed interface plane (line in 2D) is given as $ax + by + cz + d = 0$ where interface normal $\underline{n} = [a, b, c]^T$. The

reconstruction of original/reference interface means determining the components of interface normal $\underline{n}$ and shortest distance of interface from cell center d. In MOF method, we find these two quantities by satisfying volume conservation (Equation (3)) and least centroid defect (Equation (4)). The centroid defect is defined as the distance between the phase centroids of the reference and actual/reconstructed interface. The two conditions are:

$$\mid F^{\text{ref}} - F^{\text{act}}(\underline{n}, d) \mid = 0, \text{ and} \tag{3}$$

$$E^{\text{MOF}}(\underline{n}, d) = \min_{\text{Eq. (3) holds}} \left\| \underline{x}^{\text{ref}}_{\text{COM}} - \underline{x}^{\text{act}}_{\text{COM}}(\underline{n}, d) \right\|_2 . \tag{4}$$

where F represent liquid volume fraction and x_{COM} is the liquid phase centroid. All the variables containing the superscript "ref" represents the variables pertaining to the original (reference) interface while those containing the superscript "act" represents the variables pertaining to the reconstructed (actual) interface. The reference interface is chosen for a fluid (either liquid/gas) based on the farthest distance of its centroid from the cell center x_{C_Ω} (where C_Ω is a computational cell inside the domain Ω), i.e.,

$$\text{Reference fluid} = \begin{cases} \text{liquid}, & \left\| x^{\text{ref}}_{\text{COM,liq}} - x_{C_\Omega} \right\| > \left\| x^{\text{ref}}_{\text{COM,gas}} - x_{C_\Omega} \right\| \\ \text{gas}, & \text{otherwise.} \end{cases} \tag{5}$$

Thus, the centroid defect is minimized for the phase with the minimal volume in the cell. The rationale behind this approach is that, the interface orientation has highest sensitivity to the centroid defect of the phase with least volume. For the purpose of illustration, Figure 1 shows a typical computational cell in 2D with the reference and reconstructed interfaces based on liquid as reference fluid. The parameter d is computed as a result of satisfying

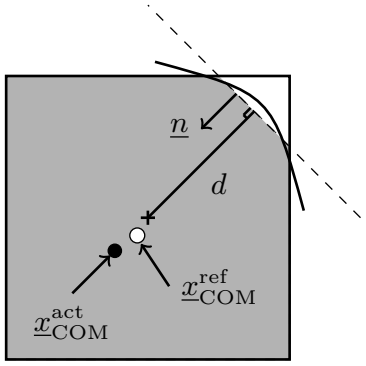

Figure 1: Computational cell with reference (solid line) and reconstructed (dashed line) interfaces and liquid centroid

the volume conservation condition (Equation (3)) upto the machine precision using Newton-Raphson method. The interface normal $\underline{n}$ is obtained from minimizing the centroid defect E^{MOF} using Gauss-Newton minimization method. It is to be mentioned that this minimization algorithm finds local minima and not the global minima. The reference liquid volume fraction F is advected by a directionally split algorithm described in [16] and the reference liquid and gas phase centroids are advected using a directionally split Eulerian Implict-Lagrangian Explicit (EI-LE) scheme. For more details, the readers are referred to Asuri Mukundan et al. [7].

The coupled level set volume of fluid (CLSVOF) method of Ménard et al. [9] is used for obtaining the level set function for interface capturing in our solver.

3.2 Interface Resolution Quality (IRQ)

The main idea of the CLSMOF method development is to use MOF only when it is necessary. This necessity is driven by presence of under-resolved liquid structures which are smaller in size than the employed mesh resolution. Thus, it is required to find and distinguish resolved and under-resolved liquid structures from one another. To this end, we propose a criteria called *interface resolution quality* (IRQ) which is expressed as

$$\text{IRQ} = \frac{1}{\Delta x \mid \kappa \mid}, \tag{6}$$

where Δx is the mesh spacing and κ is the liquid/gas interface curvature. The threshold value of IRQ determines which of the liquid structures in the domain are resolved and which are under-resolved. Based on the literature [17, 18], we decided to use the threshold value of 2.0 for IRQ. This means, for any computational cell containing a liquid phase and has a value of IRQ less than 2.0 (correspondingly, less than 8 cells along the liquid structure effective spherical diameter) would be treated as under-resolved liquid cell structure, thus, MOF will be employed for interface reconstruction. For all other IRQ values, the level set function from CLSVOF method will be used for interface reconstruction. It is to be remarked that Jemison et al. [15] used a similar criteria with a higher threshold value in their work.

4. Case Setup

A planar pre-filming airblast atomizer configuration is considered in this work. Figure 2 represents a geometry simplification of the annular atomizer used in our Direct numerical simulations (DNS). This simplified geometry is inspired from the work of Gepperth et al. [5] and Warncke et al. [6].

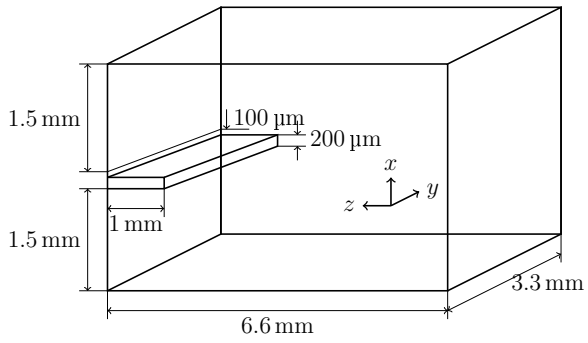

Figure 2: DNS computational domain

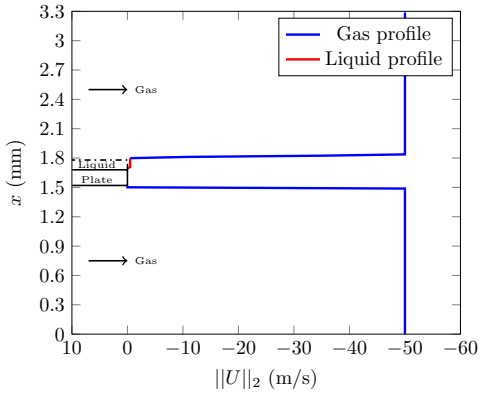

Figure 3: Velocity profile for liquid and gas phases

4.1 Operating Conditions

Fuel injection in aircraft engines are characterized by high Reynolds and Weber number. A detailed investigation of fuel injection in such highly turbulent environment is challenging using DNS. In this work, a moderate operating point is chosen with a comparitively low Reynolds and liquid film Weber number. This operating point correspond to the aircraft altitude relight conditions [19] and allows an adequate resolution of the atomization events. The operating conditions are summarized in Table 1 with channel half width $H_{\text{chw}} = 4\,\text{mm}$ and liquid thickness $h_{\text{l}} = 100\,\mu\text{m}$. The liquid fuel used in this study correspond to Shellsol D70 with a low surface tension at ambient conditions.

Table 1: Operating Conditions Summary

Non-dimensional num.	$\text{Re}_{\text{gas}} = \frac{u_{\text{gas}} H_{\text{chw}}}{\nu_{\text{gas}}} = 13333$	$\text{We}_{\text{film}} = \frac{\rho_{\text{gas}} u_{\text{gas}} h_{\text{l}}}{\sigma} = 10.69$	$M = \frac{\rho_{\text{gas}} u_{\text{gas}}^2}{\rho_{\text{liq}} u_{\text{liq}}^2} = 15.58$
Gas properties	$u_{\text{gas}} = 50\,\text{m/s}$	$\rho_{\text{gas}} = 1.2\,\text{kg/m}^3$	$\nu_{\text{gas}} = 1.5 \times 10^{-5}\,\text{m}^2/\text{s}$
Liquid properties	$u_{\text{liq}} = 0.5\,\text{m/s}$	$\rho_{\text{liq}} = 770\,\text{kg/m}^3$	$\nu_{\text{liq}} = 2.03 \times 10^{-6}\,\text{m}^2/\text{s}$
	$\sigma = 0.0275\,\text{kg/s}^2$		

4.2 Computational Setup

The air flow inlet is located each above and below the pre-filmer plate. A flat velocity profile as shown in Figure 3 with the magnitude of the mean liquid and gas phase velocity is imposed as the inlet profile. The DNS domain has been chosen in such a way that there is enough length along the downstream direction to analyze atomization but also kept as small as possible to avoid blow up of the computational cost.

The faces of the pre-filmer plate are treated as walls using the staircase immersed boundary method (SIBM). In this method, the shape of the pre-filmer plate is approximated such that it fits in the Cartesian grid lines. Thus, fluxes over the cell faces containing the solid pre-filmer plate can be computed like that for a no-slip boundary cell face. Periodic boundary conditions have been used along the $y-$direction, while outflow boundary conditions on all other directions except the liquid and gas injection $z-$plane.

A computational mesh with a mesh spacing of $\Delta x = \Delta y = \Delta z = 12.89\,\mu$m has been employed to capture the liquid droplets resulting in a total of 33.5 million cells. For the value of Reynolds number employed in this study, the Kolmogorov length scale was found to be $\eta = 12\,\mu$m. Thus, based on [20], the required minimum grid spacing is $\Delta x_{\min} \approx 25\,\mu$m. With the grid resolution used in this work, it can be said that we will be able to resolve the predominant scales of motion. The simulation has been run upto a physical time of 14 ms on 1024 processors in CRIANN supercomputing facility [21]. The data have been written in the disk about every 34 µs.

4.3 Experimental Comparison

In order to validate the results from DNS, we will be comparing with the experimental data from the work done at the Institut für Thermische Strömungsmaschinen (ITS) at Karlsruhe Institut für Technologie. The experiments have been performed for 30 s of physical time and double frame images (in both $y-z$ and $x-z$ plane views) that are phase shifted by 10 µs. Each droplet in the double image was considered for the computation of statistics. To statistically derive robust results for the ligament and droplet sizes, an efficient algorithm based on the particle and ligament tracking velocimetry developed by Müller [22] with an extension to Depth of Field (DoF) correction to increase the measurement accuracy was used. For more details on the measurement and post-processing techniques employed in the experimental work, the reader is referred to [5, 6].

5. Results and Discussion

In this section, the results from post-processing the DNS data are presented. First, the qualitative results of the flow visalisation are presented. Then the quantitative results on the droplets and ligaments are presented.

5.1 Qualitative results

Figure 4 shows several instantaneous snapshots of the flow visualization. The breakup process is as follows: waves are generated on top of the pre-filmer plate (c.f Figure 4b) that actually causes shearing in the liquid layer which then forms a liquid reservoir at the trailing edge of the pre-filmer plate. From this reservoir, thin sheets and long ligaments of liquid are formed (c.f. Figure 4b) which then develops holes in them (c.f. Figure 4c) since the surface tension cannot counteract the disintegration process. The holes penetrate the sheet causing breakup into small droplets whose diameters are of the order of thickness of the sheet (c.f. Figure 4c) and long ligaments breaks up into bulgy and medium-sized droplets (c.f. Figure 4d). This observation is consistent to the torn sheet breakup regime described in Fernández et al. [23] for the operating point in this work. No dewetting of the plate was observed in the simulations. Moreover, the flapping of the liquid sheet (observed in side view $x-z$ plane) was found to be asynchronuous to the atomization.

5.2 Quantitative results

The quantitative data obtained from DNS has been post-processed and analyzed in order to compare with the experimental results. This section first presents the post-processing techniques employed for the DNS data that is consistent to that of the experiments. This is then followed by the characterization of the droplets and ligaments that include presentation of their probability distribution and also their mean values.

5.3 Post-processing Techniques

The post-processing and analysis of the DNS data is split into two parts: analysis of droplets and analysis of accumulated liquid ligaments at the trailing edge of the pre-filmer plate.

In order to determine the probability distribution of the droplets in the domain, a connected component labelling (CCL) algorithm is used. This algorithm finds list of all the liquid structures in the domain at a given time instant by using a 8-cell neighbor connectivity search for liquid presence. This list contains all the attributes of the liquid

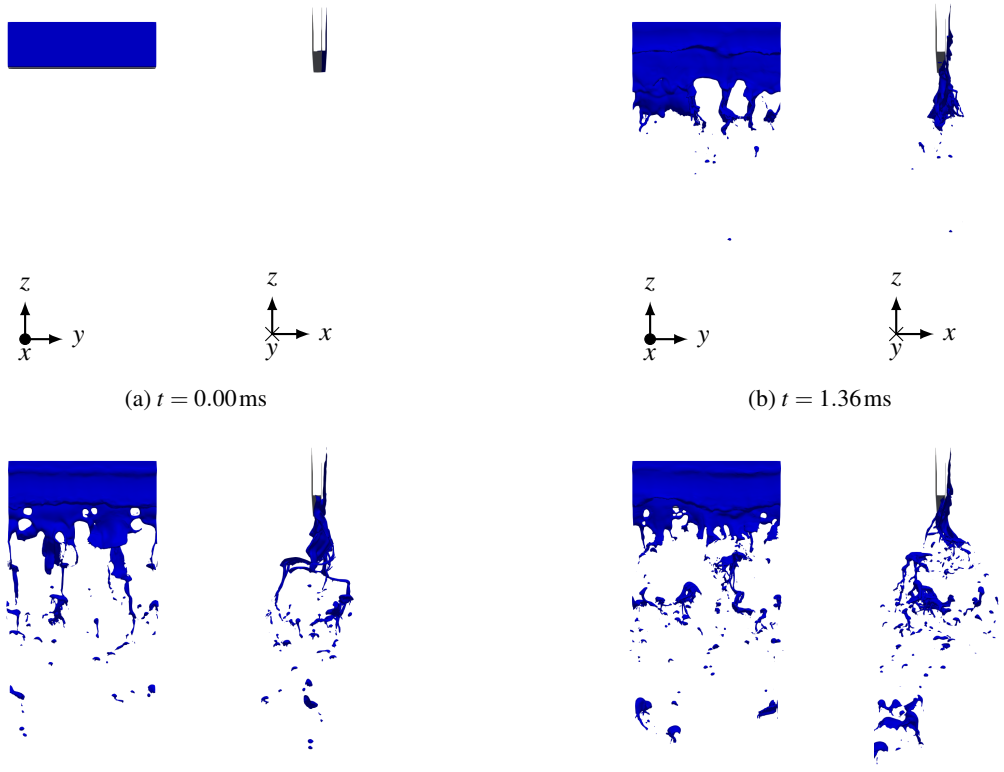

(a) $t = 0.00\,\text{ms}$ (b) $t = 1.36\,\text{ms}$

(c) $t = 5.79\,\text{ms}$ (d) $t = 8.13\,\text{ms}$

Figure 4: Atomization of liquid fuel at the trailing edge of pre-filmer plate forming ligaments and droplets

structures such as velocity components, surface area, diameter, and volume. It is to be remarked that the liquid droplet structure diameter is derived from its volume with the assumption that liquid structure is spherical.

The extraction of results for the liquid ligaments accumulated at the trailing edge of the pre-filmer plate such as ligament lengths, breakup length, and streamwise velocity are not straightforward and is challenging. To this end, we have used an algorithm that is split into four steps. First, the 3D DNS data (c.f. Figure 5a) is reduced to a 2D data analogous to the shadowgraphy images by assigning label value of 0 (for gas) and 1 (for liquid) to each cell with zero and non-zero liquid volume fraction respectively. Second, these label values are summed up along cross-stream $x-$direction to generate a projected top view ($y-z$ plane view) (c.f. Figure 5b). Any cell in this top view with a summed label value greater than 1 indicates presence of liquid in this view. Third, a CCL algorithm is applied for these summed up label values to identify the biggest liquid structure, i.e., the accumulated liquid at the trailing edge of pre-filmer plate (c.f. Figure 5c). Finally, the 1D interface contour is identified that characterizes the interface of this accumulated liquid (c.f. Figure 5d). This procedure has been applied to every time step since the first breakup event has occurred.

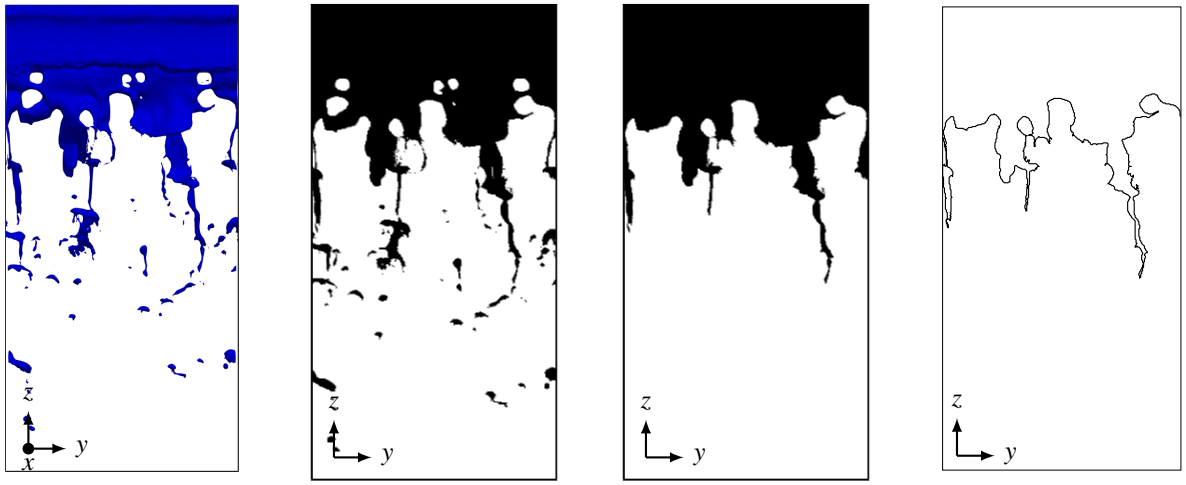

(a) 3D DNS data (b) 2D Projected DNS data (c) Biggest liquid structure (d) 1D phase interface

Figure 5: Reduction of 3D to 1D data for computing ligament characteristics for $t = 5.79\,\text{ms}$

5.3.1 Droplet characterization

With the post-processing technique described above, first the droplet characteristics are extracted from the DNS. These include droplet diameter and droplet streamwise velocity (w_z) distributions shown in Figure 6. The liquid packets are obtained for each time step from the whole DNS domain. In order to have single count of a liquid packet/droplet, we developed an algorithm that tracks the position of each droplet between adjacent time steps (t^n and t^{n+1}, for example) and adds to the list of droplets for distribution plot only when it goes out of the domain at t^{n+1}. The smallest diameter measured in the experiment was 15 µm, so, the droplet distribution from the simulation is computed keeping this smallest droplet diameter. It can be observed that a satisfactory agreement between the simulation and experiments is observed with under-prediction from the simulation. A profile similar to that of the experiments is observed from the simulations. Droplet diameters upto 330 µm are found from the DNS. As seen in Section 5.1, medium sized and bulgy droplets are found thus owing to the higher peak for the medium sized droplets around 77 µm. This shows that the ligament breakup is dominant over sheet breakup in the simulations. This observation could also be attributed to the flat velocity profile chosen in our study for the liquid and gas phase. The investigation of the effect of inlet velocity profile on the droplet characteristics is considered as future work in our project.

The droplet velocity distribution shown in Figure 6b displays a good agreement with the mean velocity from the experiment measured as 14.5 m/s while that from the simulation is 14 m/s. Moreover, the trend in the profile of the distribution function is similar to that of the experiments.

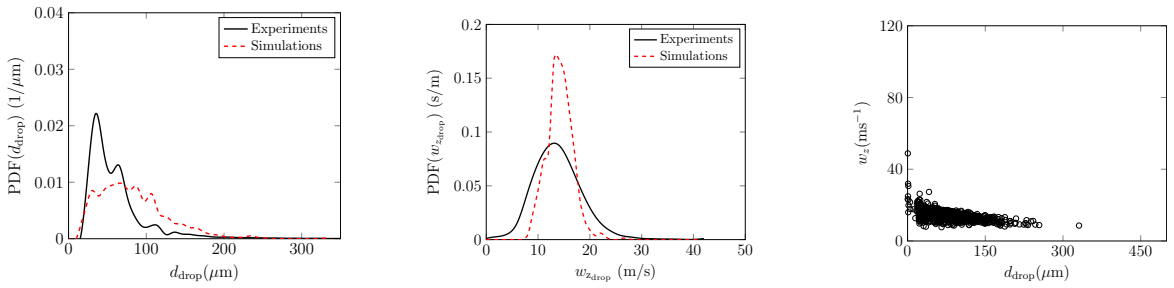

(a) Droplet size distribution (b) Droplet velocity distribution (c) Scatter plot of droplet velocity and diameters

Figure 6: Characterization of droplets

A total of 839 droplets were identified after post-processing the DNS data for simulations run upto 14 ms. In contrast, about 38 000 droplets were identified from the experiments for a measurement duration of 30 s. To get deeper

insights into the droplet properties, a scatter plot of the streamwise droplet velocity and droplet diameter is shown in Figure 6c for all droplets. It can be seen that there are small droplets with high velocity between 35 m/s and 50 m/s are present in the domain. This observation is consistent with the experiments [6]. Finally, the Sauter Mean Diameter (SMD) computed from the DNS is 130.13 µm. This is in very good agreement with the value found from the experiment of 154.8 µm.

5.3.2 Ligament characterization

The ligaments are formed in irregular shapes at the trailing edge of the pre-filmer plate. The characterization of these ligaments are performed using computation of ligament lengths and breakup length. To this end, the accumulated liquid at the trailing edge of pre-filmer plate is under focus. The method explained in Warncke et al. [6] is used for the experiments while the technique employed for post-processing our DNS data is explained below.

A single ligament length l_{lig} is defined, within this work, as the distance between the ligament peak and the trailing edge of the pre-filmer. To compute the ligament length for a single time step, the 1D phase interface contour (c.f. Section 5.3) is used. The maximum dip in this 1D phase interface along the downstream direction is used for identifying the ligaments. The critical point in this identification is to compute the true ligament by eliminating the effect of the wrinkling in the interface. For this reason, following [6], we use a criterium of 50 µm distance between the adjacent minima and maxima measured along the streamwise $z-$direction is kept as a threshold to eliminate this effect and obtain a more global behavior. This is shown in Figure 7 with the squares indicating the location of the maximum dip in the interface in the downstream direction. The length of these resulting maximum dips (called true ligament lengths hereon) are computed from the edge of the pre-filmer plate. The breakup length l_{breakup} is then defined as the mean of these true ligament lengths over all time steps.

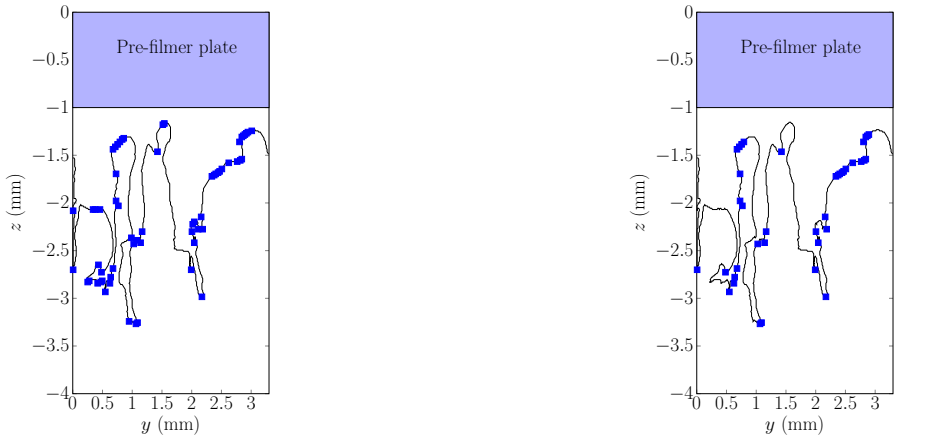

(a) All identified maxima

(b) True maxima after 50 µm criterium

Figure 7: Detection of phase interface peak (blue squares) for ligament length computation

Based on these computations, the breakup length from the DNS is found to be $l_{\text{breakup}} = 1.6\,\text{mm}$ while the experimental value measures 3.2 mm. The breakup length from the simulations are smaller in magnitude albeit of the same order as that of the experimental value. Per the study of Sauer et al. [24], when the breakup length is computed as the maximum of all the ligament lengths, the result from our simulation is 3.74 mm which is only a little over-prediction in comparison to the experiments. In experiments, a small amount of ligaments whose lengths measures greater than the length of the streamwise direction in the DNS are observed which results in a greater breakup lengths. Furthermore, a total of 12 201 ligaments have been identified from the DNS post-processing while 13 000 ligaments from the experiments.

To get a better understanding, frequency distribution of ligament length is computed and shown in Figure 8. It can be seen that the peak of this ligament length distribution is shifted towards smaller lengths. This is due to three reasons: first, no ligaments measured from our simulations reaches the outlet of the domain; second, there was greater time period for the sampling in the experiments, and therefore, a higher amount of samples compared to the simulations; and third, the field of view of measurement for experiments are larger than that of the DNS, thus, longer ligament

lengths that are greater than the length of the streamwise direction of the DNS domain are observed. Furthermore, these under-predictions could be attributed to the insufficiency of the mesh resolution to capture the breakup events.

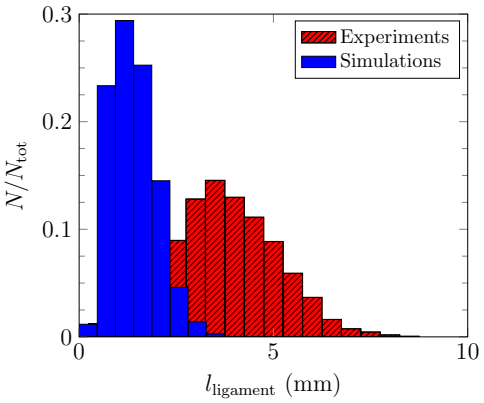

Figure 8: Ligament length frequency distribution

6. Conclusions

We have simulated a planar pre-filming airblast atomization using DNS and CLSMOF method of interface capture in the context of multiphase flows. A detailed comparison of the different droplet and ligament characteristics have been presented and compared with the experimental results. A very good agreement was shown for the Sauter Mean Diameter (SMD) measure. A good agreement has been observed for the droplet velocity and a satisfactory agreement has been observed for the droplet diameters. The ligament lengths were extracted from the DNS data using the 1D phase interface reduced from the 3D DNS data. The comparisons with the experiments yielded satisfactory agreement on the ligament breakup length. This is attributed to the fact that experiments were run for a longer period of time and had larger field of view for measurement than the DNS.

In future, it is envisaged to perform DNS for finer mesh resolution to capture the breakup physics and capture the small droplets. Additionally, usage of a bigger DNS domian and a more realistic velocity profile for the phases such as a fully developed turbulent channel flow profile are considered in the next studies.

7. Acknowledgements

The funding for this project from the European Union's Horizon 2020 research and innovation programme under the Marie Skłodowska-Curie grant agreement N° 675676 is gratefully acknowledged. The computing time at CRIANN (Centre Régional Informatique et d'Applications Numériques de Normandie) under the scientific project No. 2003008 is also gratefully acknowledged. The authors would like to thank Prof. Dr. Jean-Bernard Blaisot for graciously sharing his algorithm of finding the 1D interface contour. The authors wish to thank Prof. Rainer Koch and his group at Karlsruhe Institut für Technologie (KIT) for graciously sharing their experimental data.

References

[1] A. H. Lefebvre and D. Miller, The development of an Air Blast Atomizer for gas turbine application, tech. rep. Report No. AERO No. 193, The College of Aeronautics Cranfield, 1966.

[2] U. C. Bhayaraju and C. Hassa, Planar liquid sheet breakup of prefilming and nonprefilming atomizers at elevated pressures, Atomization and Sprays 19 (2009) 1147–1169.

[3] A. K. Jasuja, Behaviour of aero-engine airblast sprays in practical environment, Proceedings of the 10th ICLASS, July 22nd-26th, Chicago, USA (2006).

[4] C. Bilger and R. Stewart Cant, Mechanisms of Atomization of a Liquid-Sheet: A Regime Classification, Proceedings of the 27th Annual Conference on Liquid Atomization and Spray Systems, 4-7 September 2016, Brighton, UK (2016).

[5] S. Gepperth, A. Müller, R. Koch, and H.-J. Bauer, Ligament and Droplet Characteristics in Prefilming Airblast Atomization, Proceedings of the ICLASS 2012, 12th Triennial International Conference on Liquid Atomization and Spray Systems, Heidelberg, Germany, September 2-6, 2012 (2012).

[6] K. Warncke, S. Gepperth, B. Sauer, A. Sadiki, J. Janicka, R. Koch, and H.-J. Bauer, Experimental and numerical investigation of the primary breakup of an airblasted liquid sheet, International Journal of Multiphase Flow 91 (2017) 208–224.

[7] A. Asuri Mukundan, T. Ménard, A. Berlemont, and J. C. Brändle de Motta, Interface reconstruction method for multiphase flows in under-resolved regions, 10th International Conference on Computational Fluid Dynamics ICCFD10 2018, 9–13 July, Barcelona, Spain (2018).

[8] A. Asuri Mukundan, T. Ménard, A. Berlemont, and J. C. Brändle de Motta, Numerical study of interface reconstruction method in under-resolved regions of the flow for liquid jet primary breakup, Proceedings of the 14th ICLASS, July 22nd-26th, Chicago, USA (2018).

[9] T. Ménard, S. Tanguy, and A. Berlemont, Coupling level set/VOF/ghost fluid methods: Validation and application to 3D simulation of the primary break-up of a liquid jet, International Journal of Multiphase Flow 33 (2007) 510–524.

[10] S. Tanguy and A. Berlemont, Application of a level set method for simulation of droplet collisions, International Journal of Multiphase Flow 31 (2005) 1015–1035.

[11] G. Vaudor, T. Ménard, W. Aniszewski, M. Doring, and A. Berlemont, A consistent mass and momentum flux computation method for two phase flows. Application to atomization process, Computers and Fluids 152 (2017) 204–216.

[12] M. Sussman, K. M. Smith, M. Y. Hussaini, M. Ohta, and R. Zhi-Wei, A sharp interface method for incompressible two-phase flows, Journal of Computational Physics 221 (2007) 469–505.

[13] R. Fedkiw, T. Aslam, B. Merriman, and S. Osher, A Non-oscillatory Eulerian Approach to Interfaces in Multimaterial Flows (the Ghost Fluid Method), Journal of Computational Physics 152 (1999) 457–492.

[14] V. Dyadechko and M. Shashkov, Reconstruction of multi-material interfaces from moment data, Journal of Computational Physics 227 (2008) 5361–5384.

[15] M. Jemison, E. Loch, M. Sussman, M. Shashkov, M. Arienti, M. Ohta, and Y. Wang, A Coupled Level Set-Moment of Fluid Method for Incompressible Two-Phase Flows, Journal of Scientific Computing 54 (2013) 454–491.

[16] G. D. Weymouth and D. K.-P. Yue, Conservative Volume-of-Fluid method for free-surface simulations on Cartesian-grids, Journal of Computational Physics 229 (2010) 2853–2865.

[17] M. Gorokhovski and M. Herrmann, Modeling Primary Atomization, Annual Review of Fluid Mechanics 40 (2008) 343–366.

[18] J. Shinjo and A. Umemura, Simulation of liquid jet primary breakup: Dynamics of ligament and droplet formation, International Journal of Multiphase Flow 36 (2010) 513–532.

[19] T. Mosbach, R. Sadanandan, W. Meier, and R. Eggels, Experimental Analysis of Altitude Relight Under Realistic Conditions Using Laser and High-Speed Video Techniques, Proceedings of the ASME Turbo Expo 2010: Power for Land, Sea, and Air, Volume 2: Combustion, Fuels and Emissions, Parts A and B, Glasgow, UK, June 14–18, 2010 (2010).

[20] S. B. Pope, Turbulent Flows, Cambridge University Press, 2000.

[21] *Utilisation du Cluster Myria, CRIANN Supercomputing Facility*, Centre Régional Informatique et d'Applications Numériques de Normandie, 2018.

[22] A. Müller, Experimentelle Untersuchung des Zerstäubungsverhaltens luftgestützter Brennstoffdüsen bei oszillierenden Strömungen, PhD thesis, Institut für Thermische Strömungsmaschinen (ITS), Karlsruhe Institut für Technologie, 2015.

[23] V. G. Fernández, P. Berthoumieu, and G. Lavergne, Liquid sheet disintegration at high pressure: An experimental approach, Comptes Rendus Mécanique 337 (2009) 481–491.

[24] B. Sauer, A. Sadiki, and J. Janicka, Embedded DNS Concept for Simulating the Primary Breakup of an Airblast Atomizer, Atomization and Sprays 26 (2016) 187–217.